Article

Photo-Fenton Catalyzed by Cu_2O/Al_2O_3: Bisphenol (BPA) Mineralization Driven by UV and Visible Light

Oscar Olea-Mejia [1,*] , Sharon Brewer [2], Kingsley Donkor [2], Deysi Amado-Piña [1] and Reyna Natividad [1,*]

1   Centro Conjunto de Investigación en Química Sustentable UAEM-UNAM, Carretera Toluca-Atlacomulco Km 14.5, San Cayetano, Toluca 50200, Mexico
2   Department of Chemistry, Thompson Rivers University, Kamloops, BC V2C 0C8, Canada
*   Correspondence: oleaoscar@yahoo.com.mx (O.O.-M.); rnatividadr@uaemex.mx (R.N.)

Abstract: This work aimed to demonstrate Cu_2O/Al_2O_3 as a catalyst of the photo-Fenton process in the UV and visible spectra. Cu_2O nanoparticles were synthesized by laser ablation in liquid and supported on Al_2O_3. The catalytic activity of the resulting solid was assessed in the mineralization of bisphenol A (BPA). The studied variables were type of Al_2O_3 (α and γ), Cu content (0.5 and 1%), and H_2O_2 concentration (1, 5, and 10 times the stoichiometric amount). The response variables were BPA concentration and total organic carbon (TOC) removal percentage. The presence of Cu_2O nanoparticles (11 nm) with an irregular sphere-like shape was confirmed by transmission electron microscopy (TEM) and their dispersion over the catalytic surface was verified by energy-dispersed spectroscopy (EDS). These particles improve ·OH radical production, and thus a 100% removal of BPA is achieved along with ca. 91% mineralization in 60 min. The BPA oxidation rate is increased one order of magnitude compared to photolysis and doubles that for H_2O_2 + UV. An increase of 40% in the initial oxidation rate of BPA was observed when switching from α-Al_2O_3 to γ-Al_2O_3. 4-hydroxybenzaldehyde, 4-hydroxybenzoic acid, acetaldehyde, and acetic acid are the BPA oxidation by-products identified using LC/MS and based on this a reaction pathway was proposed. Finally, it was also concluded that the synthesized catalyst exhibits catalytic activity not only in the UV spectrum but also in the visible one under circumneutral pH. Therefore, Cu_2O/Al_2O_3 can be recommended to conduct a solar photo-Fenton reaction that can degrade other types of molecules.

Keywords: BPA degradation; photo-Fenton; nanocomposite catalysts; bisphenol A mineralization; solar photo-Fenton

1. Introduction

Bisphenol A (BPA) is ubiquitous in the environment. Potential sources of human exposure to bisphenol A are air, water, soil, sediments, indoor dust, and human tissues. Bisphenol A is an emerging environmental contaminant. The continuous release of bisphenol A into the environment results in the continuous exposure of both plant and animal life to it. Furthermore, BPA has been determined to be an endocrine disruptor chemical, potentially associated with numerous diseases such as breast cancer, infertility, cognitive dysfunction, diabetes, cardiovascular diseases, and obesity. As a response to these concerns, several countries have banned the use of BPA in various consumer products. The abovementioned effects of BPA on human health and the environment prompted us to choose it as the research object in the present work and develop the method presented here, which can be used to remove or minimize its presence [1,2].

There are various techniques to remove pollutants from contaminated streams; these include adsorption [3,4], biodegradation, and thermal destruction, among others. However, these methods also have important disadvantages, such as only transferring the pollutant from one material to another, high energy requirements, and slow process. In this context, advanced oxidation processes (AOPs) are known to be highly efficient in removing

organic contaminants from water, the Fenton process being one that has been extensively studied [5]. However, the Fenton reaction takes place in highly acidic conditions, and iron salts are dissolved to produce the desired ·OH radicals. Evidently, the disadvantages of this technique are the loss of the iron catalyst (homogeneous catalysis) as well as the need to reverse the pH to an acceptable level after the reaction. This is usually conducted by the addition of HCl, which indicates a new problem—the increase of purification cost.

Therefore, different AOPs have been developed to overcome these disadvantages, including ozonation [6–8], heterogeneous catalysis/photocatalysis [9,10], bioprocesses [11–13], and Fenton-like reactions [14–16]. Among these methods, the heterogeneous photo-Fenton-like is a promising one. It has the advantages of re-using catalysts and can be conducted at circumneutral pH. Here, the generation of the ·OH radicals is due to the presence of H_2O_2, UV light, and the metal ion that is capable of facilitating the radical production.

The degradation of bisphenols using Fenton-like processes has been studied extensively in recent years, and several methods have been proposed, including sono-photo-Fenton [17] and photo-Fenton using UV [18–24] and visible radiation [10,25,26]. Furthermore, the use of metallic nanoparticles in Fenton-like reactions has also been studied recently, with iron being the most-used metal [6,8,15,27–33]. Copper has also been used but to a much lesser extent [34,35], and its use in the degradation of bisphenols has been barely assessed [18,36]. Therefore, copper was elected in this work because of its potential as a Fenton-like reactant and due to the very little information regarding its use in the degradation of bisphenols.

Metallic and Cu oxide nanoparticles can be produced by several methods. In this work, Cu_2O nanoparticles were produced via laser ablation in liquid (LAL). LAL is a physical method that can produce nanoparticles from a pure metal target immersed in a liquid medium. In short, a high-energy pulsed laser is focused on the surface of the target, the material is abruptly heated, and plasma is formed. Subsequently, the plasma condenses in the form of nanoparticles inside the liquid [37]. The main advantage when using LAL is that the obtained nanoparticles are free from any chemical by-products [38,39]. This is relevant to catalytic applications because the surface contamination-free nanoparticles are readily available to interact with the chemical species in the reaction of interest.

This work aimed to investigate the effect of the amount of H_2O_2 and the amount of Cu incorporated in the catalysts in the degradation of BPA via a photo-Fenton-like reaction using two types of commercially available Al_2O_3. This is a well-known catalytic support that is relatively low-cost, with no environmental issues. From an engineering point of view, the support of nanoparticles is desirable to ease the catalyst separation. Other Cu composites have been used successfully to this purpose [18].

2. Materials and Methods

2.1. Cu Nanoparticle Preparation and Characterization

A Continuum Surelite II laser system was used at a wavelength of 1064 nm, pulse duration of 6 ns, and repetition rate of 10 Hz. The metal used was a 2.5 cm diameter Cu target (99.99% purity, J.K. Lesker Co., Jefferson Hills, PA, USA). The liquid medium was deionized water. The full procedure has already been published in previous works. In short, 5 mL of water was added to a Pyrex glass containing the Cu target and irradiated for the time necessary to produce the required amount of Cu nanoparticles (about 20 min). The energy output from the laser system was 90 mJ/pulse. The amount of nanoparticles was calculated from the weight difference of the target before and after the laser ablation process. A JEOL JEM-2100 transmission electron microscope (TEM) was used to study the size and shape of the nanoparticles. The same equipment was used to perform high-resolution TEM (HRTEM) to elucidate the crystal structure and metallic state of the nanoparticles.

2.2. Catalyst Preparation and Characterization

Two types of alumina (Al_2O_3) were used in this work to study the possible effects of the crystalline phase and the size and shape of the alumina powder on BPA degradation

efficiency. Powders of α-Al$_2$O$_3$ and γ-Al$_2$O$_3$ (Sigma Aldrich, Burlington, MA, USA, 99% purity, 1–10 μm particle size) were used. Both types of alumina were treated prior to the addition of the nanoparticles with a solution of 1M NaOH (Sigma-Aldrich) at 60 °C for 1 h to improve the interaction with the Cu nanoparticles. After that, the alumina was dried and added to the Cu nanoparticle colloid and stirred for 1 h. Finally, the water was evaporated at 80 °C to obtain the dried Cu/Al$_2$O$_3$. The Cu concentrations used in this study were 0, 0.5, 1, and 2% weight percentages. The catalysts were studied using scanning electron microscopy (SEM), and a JEOL JSM-6510LV with an energy-dispersive X-ray spectroscopy (EDS) probe attached to it to confirm the presence of the Cu nanoparticles on the surface of the catalyst.

2.3. BPA Degradation Procedure

The BPA degradation was studied using a photo-Fenton-like reaction in an annular batch reactor with 50 mL of reaction volume. The UV irradiation was performed with a monochromatic lamp with an emission of 254 nm that was placed at the center of the reactor. All the reactions were carried out at a constant temperature of 26 °C, controlled with a water bath. The pH was not adjusted at any time and the initial pH was 6.7. The amount of catalyst was 10 mg for all experiments, and only the Cu nanoparticle concentration in the catalyst was varied, as mentioned above. The catalyst was added to the BPA solution (initial BPA concentration = 50 mg/L) and dispersed throughout the reaction via magnetic stirring. Finally, hydrogen peroxide was added to the reaction system right before the UV lamp was turned on. The amount of peroxide was varied by 1, 5, and 10 times the stoichiometric amount according to the total BPA mineralization reaction.

To establish the activity of the catalyst under visible light, the same aforementioned procedure was followed, but instead of using a 254 nm wavelength lamp, the reactor was surrounded by 4 lamps emitting light with a wavelength λ > 400 nm; 3 were placed at the perimeter of the reactor while a fourth one was placed on top of it. The lamps were TL5 Essential 14W/840, Philips Lighting.

2.4. Analytical Methods

Aliquots were taken from the reactor at regular times and centrifuged in capillary electrophoresis (CE) vials to gather the amount of catalyst in the bottom of the vial. It is important to mention that a test reaction with no UV light (only hydrogen peroxide and catalyst) was performed and no BPA degradation was registered over 1 h of reaction; therefore, it is safe to assume that even though there might be a very small amount of catalyst in the extracted aliquots there was no reaction taking place during the analytical procedures.

Capillary electrophoresis (CE) was used to study the degradation of BPA. A Beckman P/ACE System MDQ capillary electrophoresis unit was used for all CE analysis. A polyimide-coated silica capillary (50 mm long, 50 μm inner diameter) was used inside a cartridge configured for UV detection. BPA was detected via direct absorbance at 214 nm, 25 kV normal polarity, and a constant temperature of 25 °C. Before each sample injection, the capillary was rinsed with a 0.1 M NaOH solution for 5 min, with deionized water for 5 min, and with the run buffer for 8 min. The run buffer was a sodium dodecyl sulfate—tetrahydrate sodium borate (20 mM–60 mM, respectively) aqueous solution with a pH of 9.5.

Total organic carbon (TOC) measurements were performed after 20, 40, and 60 min of reaction in all cases to determine the mineralization percentage reached in each case. A TOC-VCSH analyzer (Mendel Scientific, Houston, TX, USA) was used for this purpose. The samples were sparged for 2 min with dried air to remove inorganic CO$_2$ from the ambient prior to the catalytic oxidation at 680 °C.

Liquid chromatography coupled with mass spectroscopy (LC/MS) was used to determine the possible oxidation intermediates at the end of the BPA degradation reactions. For this purpose, an HPLC system (Agilent Series 1200) was used, coupled with an LC/MS Q-TOF mass spectrometer (Agilent 6530) equipped with an electrospray ionization (ESI)

source (gas temperature, 350 °C; drying gas, 8 L/min; nebulizer, 10 psig; sheath gas temperature, 350 °C; sheath gas flow, 8 L/min; Vcap, 3500 V). The analyses were carried out in the positive ion mode and the mass spectra were collected between 40 and 250 m/z. A sample volume of 10 μL was injected into the liquid chromatograph with a flow rate of 0.5 mL/min. Separation was achieved in a Zorbax Extend-C18 column (Agilent, Mississauga, ON, Canada) at a constant temperature of 25 °C. The mobile phase had two components: Component A was pure LC/MC-grade water with a pH of 2 adjusted with phosphoric acid, and Component B was pure methanol. A gradient elution referred to Component B (%) was used: 0% for 15 min, 60% for 1 min, 40% for 5 min, and finally 0% for 9 min.

To determine the concentration of H_2O_2 over time, a colorimetric method was applied [40]. More details about this technique can also be found in [41]. A spectrophotometer was used to determine the absorbance of samples at 408 nm, where maximum absorbance was observed.

3. Results

3.1. Cu Nanoparticles and Catalyst Characterization

Figure 1a shows the TEM image of a typical sample of Cu_2O nanoparticles produced by LAL. The particles have an average size of 11 nm and an irregular sphere-like shape. To determine the chemical state and crystalline phase of the nanoparticles, high-resolution TEM (HRTEM), as seen in Figure 1b, and electron diffraction (Figure 1c) were performed. The interplanar distance from the HRTEM image is 0.24 nm, which can be ascribed to the 111 plane in the crystalline phase of Cu_2O according to the JPCDS 01-075-1531 card. To corroborate this, Figure 1c shows the diffraction rings that correspond to the 110, 111, 200, and 211 planes of Cu_2O. It is important to note that even though the target was pure Cu, Cu_2O nanoparticles were obtained, which means that the particles oxidize when in contact with water or air after being produced by laser ablation.
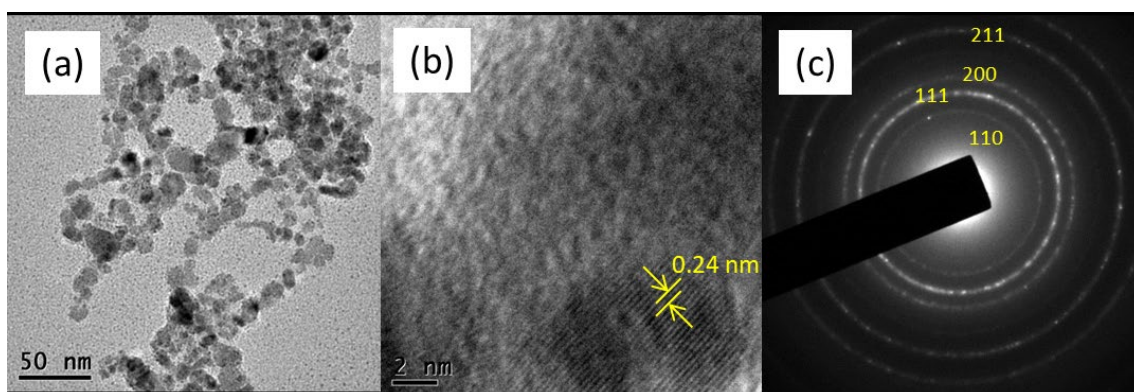

Figure 1. TEM image (**a**), HRTEM (**b**), and electron diffraction pattern (**c**) of the Cu_2O nanoparticles obtained via laser ablation in liquid.

EDS was conducted to determine the presence of Cu_2O nanoparticles on the surface of the alumina particles. Figure 2a,b show the SEM and Cu mapping for the 1% Cu/α-Al_2O_3 catalyst. As can be seen, Cu is uniformly present throughout the sample. The same observations are true for the 1% Cu/γ-Al_2O_3 catalyst (Figure 2c,d) as well as for the rest of the prepared catalyst (not shown). Having the Cu_2O nanoparticles all over the catalyst surface is very important because they can achieve their function more efficiently during the BPA degradation process, which will be further discussed in a later section.
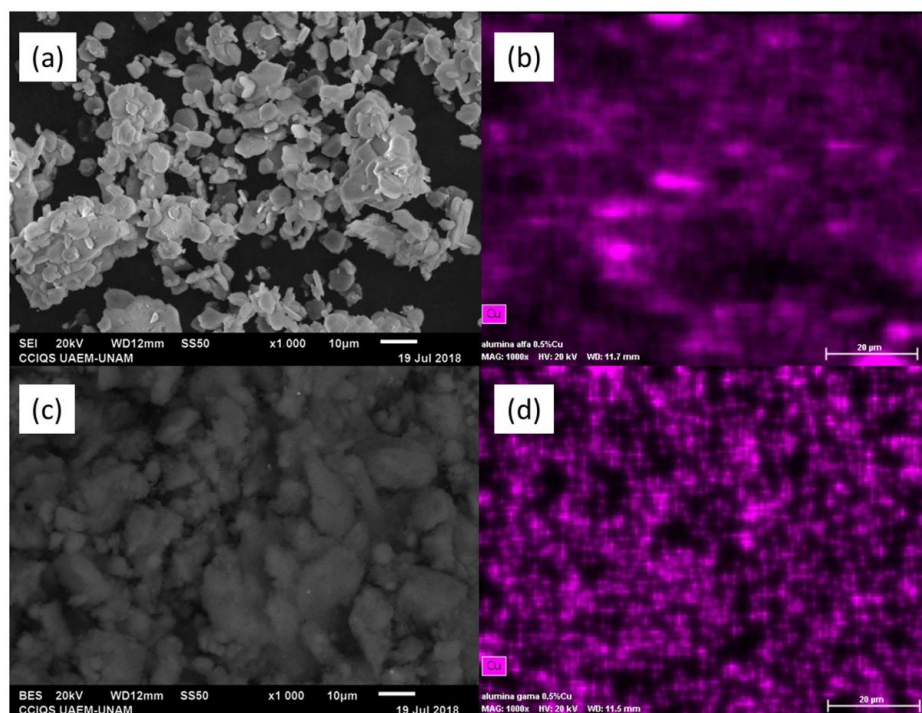
Figure 2. SEM images and Cu mapping of 1%Cu$_2$O/α-Al$_2$O$_3$ catalyst (**a**,**b**) and 1%Cu$_2$O/γ-Al$_2$O$_3$ catalyst (**c**,**d**).

3.2. BPA Degradation Results

The degradation of BPA using UV light only, UV/H$_2$O$_2$, and UV/H$_2$O$_2$/catalyst was tested to assess the possible contribution of each component in the reaction. It can be observed in Figure 3 that all the experiments led to BPA degradation, with differences in the rate and level of degradation achieved. With direct photolysis it was possible to degrade BPA to a concentration of 22.5 ppm. When H$_2$O$_2$ was added to the reaction (10 times the stoichiometric amount of the complete mineralization reaction), the BPA concentration was as low as ~1 ppm for the same reaction time (15 min), which means that almost complete degradation was reached. This considerable effect was achieved because it is known that UV light is able to form ·OH radicals from H$_2$O$_2$ (reaction 1 in Scheme 1). However, when the catalysts were added to the reaction, the complete BPA degradation occurred at shorter times. By comparing the initial BPA reaction rates ($-r_{BPA,o}$) reported in Table 1, it can be concluded that the two types of Cu$_2$O/Al$_2$O$_3$ catalyst show a similar behavior, γ-Al$_2$O$_3$ being better than α-Al$_2$O$_3$ by about 40%. This initial reaction rate corresponds to the first minute of reaction, where the hydroxyl radicals are being mainly consumed by BPA; after this reaction time, it can be observed in Figure 3 that there was a change in the slope of the BPA concentration profiles of the heterogeneous processes. This change can be ascribed to the competition of the oxidation by-products with the BPA for hydroxyl radicals. It can also be observed in Table 1 that the initial BPA oxidation rate aided by the catalyst was one order of magnitude higher than that with UV and hydrogen peroxide and with UV only. Table 1 also presents the pseudo-first order kinetic constants for each process; it can be observed that the specific rate constant for α-Al$_2$O$_3$ was about 70% higher than that obtained with UV/H$_2$O$_2$ and was more than twice that when the support was γ-Al$_2$O$_3$. Although the determination coefficient, R^2, is still reasonably good for the heterogeneous process, it can be observed that is not as good as for the homogeneous case. This could be ascribed to not incorporating in an explicit way the competition of the organic molecule with the catalyst for the photons in the applied kinetic power law model [42].
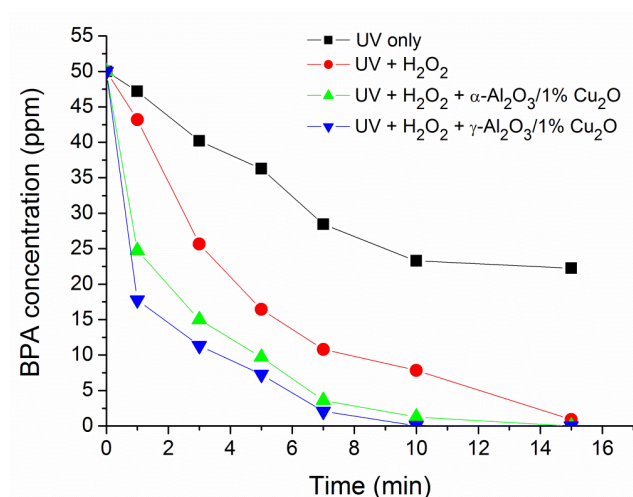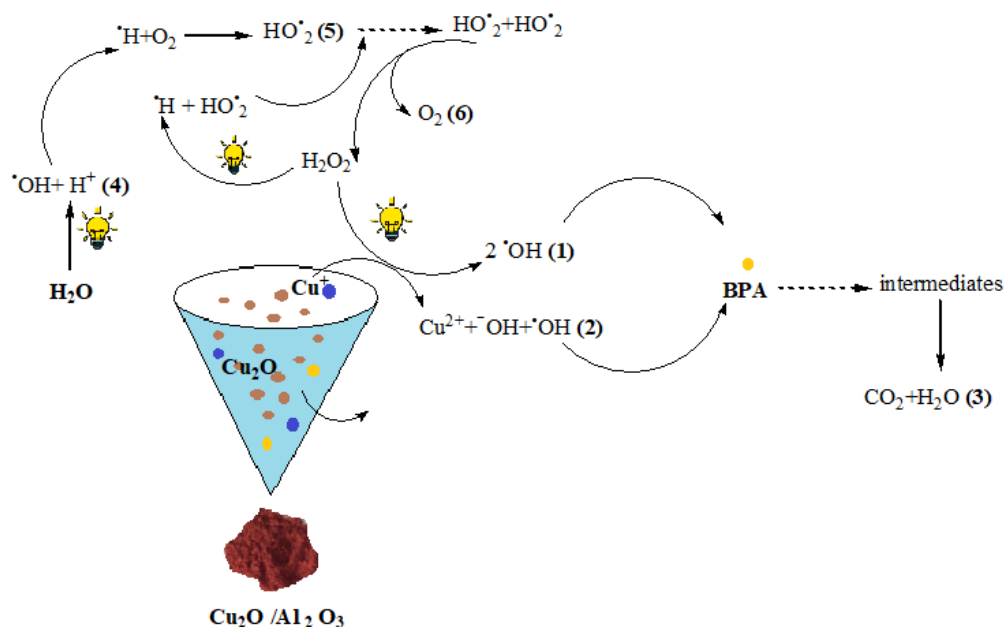
Figure 3. BPA degradation under different experimental reaction conditions.

Scheme 1. Reactions occurring at the catalyst surface and in solution in the studied photo-Fenton process catalyzed by Cu_2O/Al_2O_3.

Table 1. Percent of BPA mineralization, initial BPA oxidation rate ($-r_{BPA,o}$), pseudo-first order kinetic constant (k), and determination coefficient (R^2) under different experimental conditions.

BPA Mineralization Percentage (%)			
Time (min)	Photolysis (UV Only)	UV + H_2O_2	UV + H_2O_2 + 1% Cu_2O/α-Al_2O_3	UV + H_2O_2 + 1% Cu_2O/γ-Al_2O_3
20	2.4	17.5	19.6	24.4
40	4.7	50.5	70.1	79.6
60	7.1	80.9	86.5	90.7
Kinetic Parameters and Determination Coefficient			
$-r_{BPA,o}$ ($mol_{BPA}/L\cdot min$)	1.09×10^{-5}	1.23×10^{-5}	1.09×10^{-4}	1.4×10^{-4}
k (min^{-1})	0.074	0.1982	0.3432	0.4511
R^2	0.991	0.9969	0.9874	0.9685

In these cases, the Cu^+ ion plays a crucial role in the reaction, because the OH radicals can also be formed from the Cu ions in a similar way that Fe ions can form these radicals in a conventional Fenton reaction. Cu^+ can react with H_2O_2 to form OH and ^-OH radicals (reaction 2 in Scheme 1 [43–45]), and it is well-known that the OH radicals are the main responsible for complete mineralization of BPA through reaction 3 in Scheme 1 [46–48].

Figure 3 shows BPA degradation based solely on the BPA peak intensity measured in the CE electropherograms; however, it is not enough to determine the extent of complete mineralization of the molecule. For this purpose, Table 1 shows the TOC results for the same set of experiments. As expected, all the experiments show different mineralization values, following the tendency from Figure 3. The lowest mineralization achieved after 1 h of reaction was for the experiment when only UV light was used. This is in agreement with other reports where the activation of the BPA molecule by UV light has been suggested [48]. On the other hand, the highest mineralization was reached when the catalyst with Cu_2O nanoparticles was used. Therefore, the synthesized catalyst enhances reaction 2 (Scheme 1) in a way that not only hastens BPA degradation, but it also aids the degradation of intermediates until complete mineralization.

Figure 4 shows the consumption of hydrogen peroxide during three processes: when only adding BPA (BPA + H_2O_2); when adding BPA, UV light, and H_2O_2; and when the catalyst was added to this system. In the first case, there was no consumption of H_2O_2, and this in agreement with the BPA concentration profiles under these conditions. When the BPA + H_2O_2 was irradiated with UV light, an important consumption of H_2O_2 was observed (red dots); this was from its decomposition, as shown in Scheme 1. However, when the catalyst was added, 1500 mg/L of H_2O_2 were consumed within the system, which was significantly higher than the H_2O_2 consumed when the catalyst was absent. This is evidence of BPA oxidation occurring via the hydroxyl radicals produced in reactions 1 and 2 (see Scheme 1) as reported by [48]. Nevertheless, because of the narrow Cu_2O bandgap, a photocatalytic effect of the cupreous oxide cannot be ruled out [18]. It is worth noticing that the radicals produced are not only consumed in the degradation of BPA but also in the oxidation of the by-products.
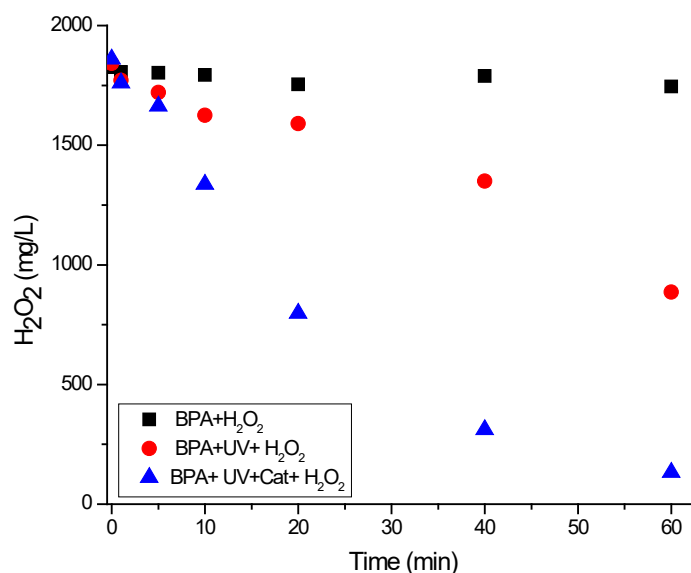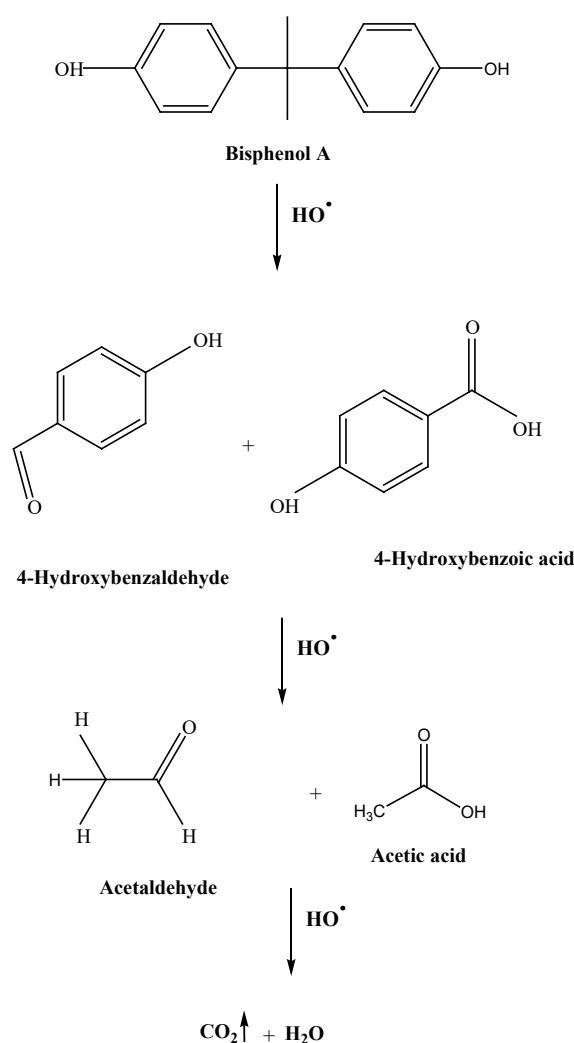

Figure 4. Hydrogen peroxide consumption profiles of BPA alone (BPA + H_2O_2), BPA and UV light (BPA + UV + H_2O_2), and by BPA, UV light, and Cu/Al_2O_3 (BPA + UV + Cat + H_2O_2).

Scheme 2 depicts a plausible BPA degradation pathway via hydroxyl radicals. The identification of acetic acid, acetaldehyde, 4-hydroxybenzaldehyde, and 4-hydroxybenzoic acid was possible by means of LC/MS.

Scheme 2. Degradation of bisphenol A by a photo-Fenton reaction catalyzed by Cu_2O/Al_2O_3: proposed reaction pathway.

Because the proposed degradation pathway is via hydroxyl radicals, it is expected to observe some similarities with other reported proposals. The first step expected is a hydroxyl radical attack of the electron-rich carbon positions. According to calculations made by [46], such positions correspond to C3 and C8. The calculated frontier density for these positions was 0.206 and 0.207, respectively. The hydroxyl radical attack of C3 may actually lead to 4-hydroxybenzaldehyde, which was identified in this work by LC/MS. It is worth pointing out that, in the context of BPA oxidation by hydroxyl radicals, this intermediate has only been identified in the photocatalytic process conducted by [46]. The hydroxyl radical attack of the electron-rich positions also leads to the appearance of the phenyl group [47] that undergoes hydroxylation to form hydroquinone. According to the literature, benzoquinone is then produced via hydroquinone dehydrogenation. Then the ring opens from further attack by hydroxyl radicals [41,47], and acetaldehyde and acetic acid appear. It is worth noting that, as in other reports, other intermediates could be present at the end of the reaction; however, they were not detected, most likely because the concentration was lower than the detection limit.

Scheme 3 depicts the three plausible structures of BPA depending on pH. This directly impacts the observed intermediates and the efficiency of the process. In this work, the initial pH was 6.7 (BPA is a weak organic acid) and it only went down to around 6.3 at the end of the experiments. Therefore, structure (A) in Scheme 3 is the one reacting in the studied system.
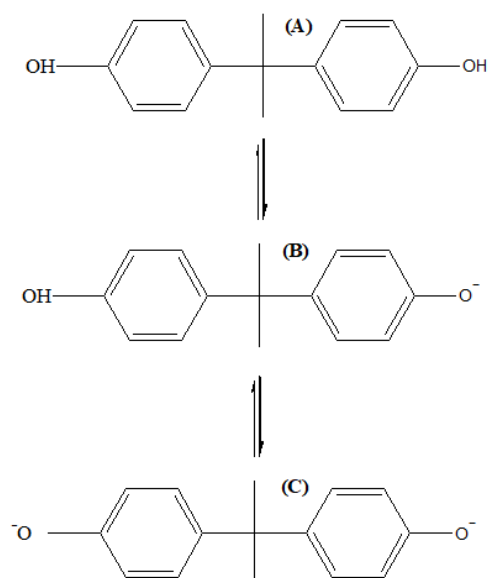
Scheme 3. BPA structures and pKa: (**A**) Neutral, (**B**) $pK_{a,1}$ = 9.59, (**C**) $pK_{a,2}$ = 10.2 [48].

3.3. Effect of H_2O_2 Concentration

From the previous results it is clear that H_2O_2 is important for the degradation of BPA, and three different concentrations of this component were tested with only UV light and no catalyst. The assessed concentrations were 1 time (1X), 5 times (5X), and 10 times (10X) the amount of H_2O_2 theoretically needed according to the stoichiometry of the complete mineralization reaction of BPA. It can be seen in Figure 5 that the lowest degradation occurred when using 1X H_2O_2. On the other hand, there seems not to be a considerable difference between the 5X and 10X cases, and it could be safely assumed that it is practically the same to use 5X or 10X of H_2O_2. However, the TOC results in Table 2 indicate that the mineralization achieved with 10X of H_2O_2 was considerably higher. This means that the rate of BPA degradation was very similar, but in the case of 10X the extra H_2O_2 was reacting to degrade the intermediates faster.
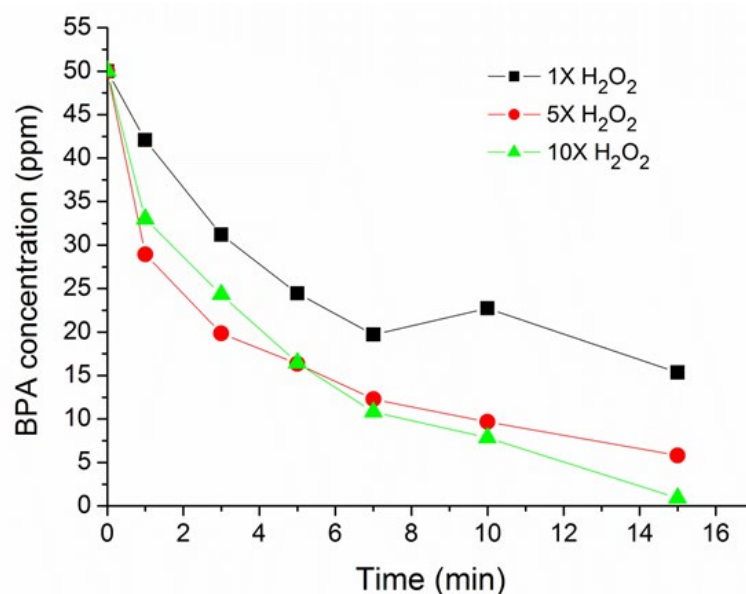

Figure 5. BPA degradation with different concentrations of H_2O_2.

Table 2. Percentage of BPA mineralization under different H_2O_2 concentrations and UV light. $C_{BPA,o}$ = 50 mg/L, pH_o = 6.7, W_{cat} = 0.0 g/L.

Time (min)	1X H_2O_2	5X H_2O_2	10X H_2O_2
20	2.3	16.8	17.5
40	15.5	25.1	50.5
60	20.6	50.0	80.9

It is worth pointing out that H_2O_2 was also being generated within the system by means of reactions 4, 5, and 6 [43,49], depicted in Scheme 1. This is plausible because of the highly energetic lamp that was being used. Figure 6 shows the H_2O_2 generation under different operating conditions. It can be observed that the accumulated amount of H_2O_2 with the lamp after 60 min was about 1.75 mg/L. It is worth clarifying that this was only part of the generated amount since there was a fraction being dissociated by UV light.
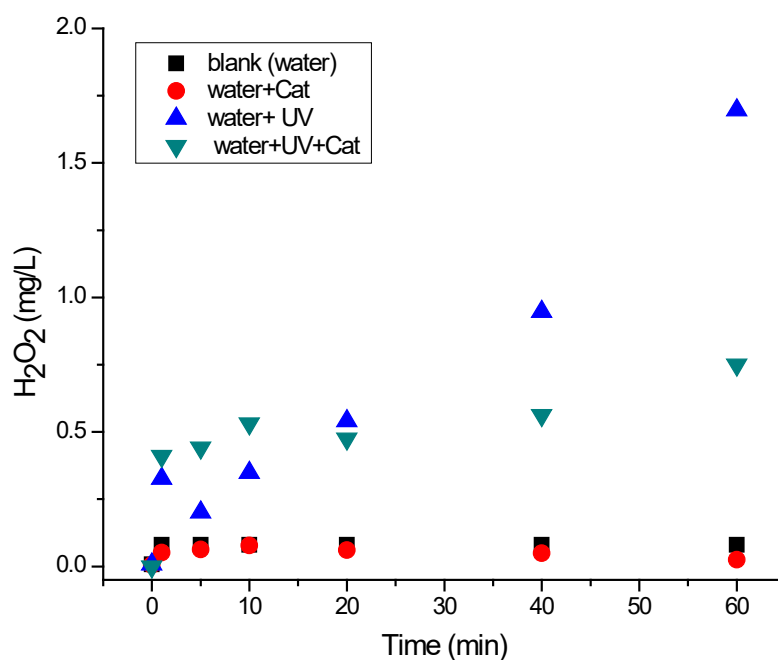

Figure 6. Production of hydrogen peroxide under different reaction conditions.

3.4. Effect of Cu_2O Concentration on the Catalyst

Based on the results from the previous section, γ-Al_2O_3 was elected as the support material to study the effect of Cu_2O concentration on the degradation of BPA. Figure 7 shows the BPA degradation for γ-Al_2O_3 catalysts with different quantities of Cu_2O added. As can be seen, when pure γ-Al_2O_3 was used without Cu_2O nanoparticles, the degradation curve was very similar to the case of H_2O_2 + UV light (Figure 5), which means that the γ-Al_2O_3 acted only as a support for Cu_2O nanoparticles and did not contribute to any catalytic function, nor hinder the reaction. On the other hand, when Cu_2O nanoparticles were added to the surface of the catalyst, a faster degradation of BPA was observed. This reinforces the hypothesis that the Cu_2O nanoparticles help degrade the BPA by creating ·OH groups via mechanisms such as the one proposed in reaction 2 in Scheme 1. Furthermore, there was no notable difference when 0.5% or 1.0% of Cu_2O was added to the catalyst, since the degradation profiles in both cases are very similar. In addition, the TOC results for these two cases show that the final mineralization after 1 h of reaction was similar (Table 3). This could be explained in terms of nanoparticle agglomeration on the catalyst surface: when loading a material with nanometric nanoparticles, there is a certain concentration where the particles start to agglomerate instead of being dispersed evenly on the surface of the

material. If this is true, then the total surface area available on the nanoparticles does not grow proportionally with the number of nanoparticles loaded to the material.
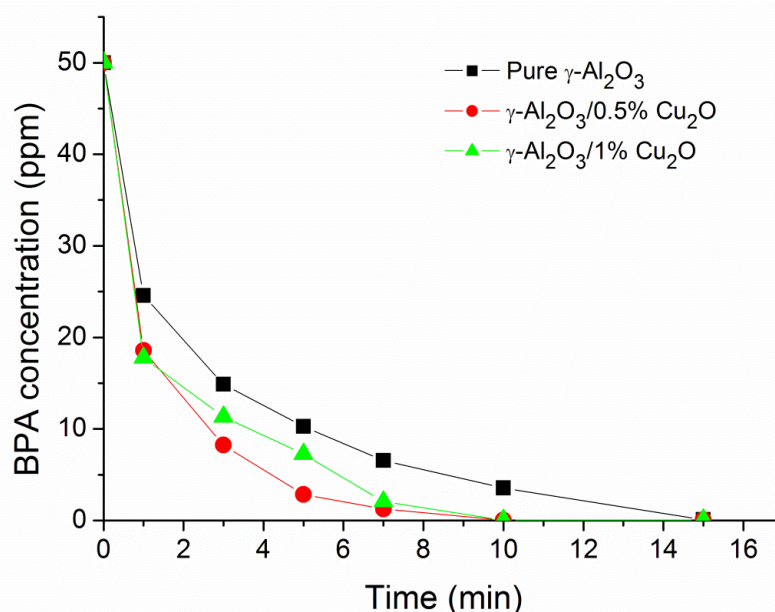

Figure 7. BPA degradation with catalysts of different Cu_2O nanoparticle concentrations.

Table 3. Percent of mineralization (TOC) of BPA by γ-Al_2O_3 with different Cu_2O content.

Time (min)	Pure γ-Al_2O_3	0.5% Cu_2O/γ-Al_2O_3	1% Cu_2O/γ-Al_2O_3
20	19.8	24.0	24.5
40	46.6	60.2	79.6
60	79.6	88.3	90.7

3.5. Effect of Radiation Source Wavelength

This variable was studied by using lamps emitting light in the visible spectrum (Vis light). Figure 8 shows the effect of different reaction variables on the TOC removal percentage after 60 min of reaction time. According to the results depicted in Figure 8, the removal of BPA by adsorption was only 5% and the removal by interaction with hydrogen peroxide was only 2.5% (gray bar). However, the TOC removal increased when Vis light was added to the system, which enhanced the TOC removal up to 18%. By comparing the results with Vis and the ones with Vis + H_2O_2, it can be concluded that dissociation of H_2O_2 does not occur readily or does not proceed at all under visible light, and therefore the addition of hydrogen peroxide alone under visible light does not improve TOC removal. On the other hand, when the catalyst and hydrogen peroxide were added to the system, the TOC removal significantly increased up to 40 and 45% for the 1% and 2 w% Cu catalyst, respectively. This is evidence of the activity of the catalyst under visible light, which is a desirable characteristic in a catalyst for the sake of sustainability. The activity of Cu_2O under visible light was expected due to its narrow bandgap (2.2 eV) [18].
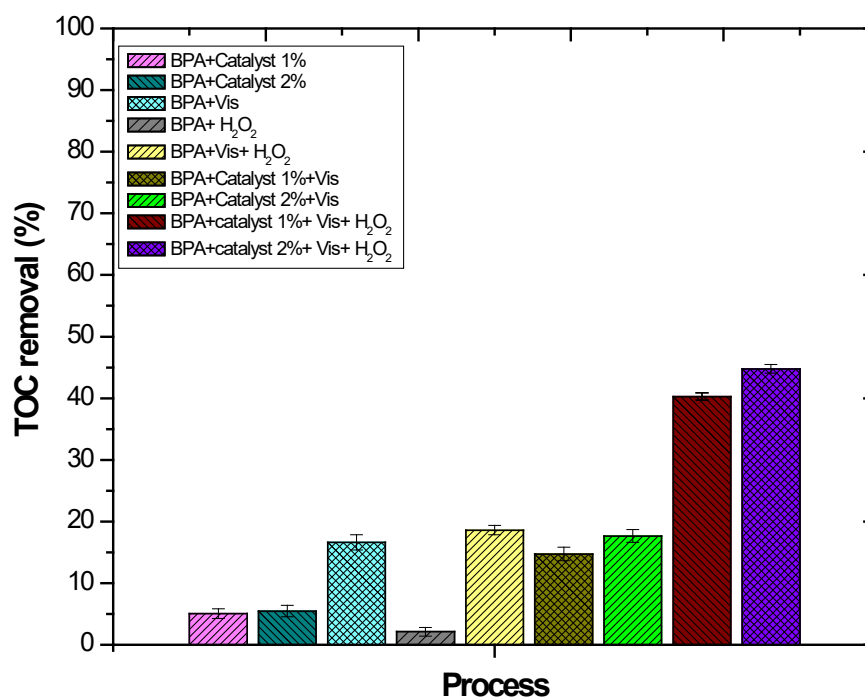
Figure 8. Effect of visible light on TOC removal percentage.

4. Conclusions

Cu$_2$O nanoparticles were obtained via laser ablation in liquid (LAL) and supported on Al$_2$O$_3$. This material catalyzes the photo-Fenton process to remove bisphenol A (BPA) under UV light as well as under visible light at circumneutral pH, and the need for acidification is eliminated. The BPA oxidation rate is one order of magnitude higher when using the catalyst than when applying only UV light and is more than twice that achieved when H$_2$O$_2$ is only dissociated by light. The BPA oxidation rate is affected by the crystalline structure of the catalyst support, Al$_2$O$_3$, and the mineralization extent is directly related to the initial H$_2$O$_2$ concentration. The highest mineralization percentage (ca. 91%) was found using 1%Cu$_2$O/γ-Al$_2$O$_3$, 10 times the stoichiometric amount of H$_2$O$_2$ at an initial pH of 6.7, and catalyst loading of 0.2 g/L.

After 1 h of treatment, the remaining compounds in solution were acetic acid, acetaldehyde, and in smaller quantities 4-hydroxybenzaldehyde and 4-hydroxybenzoic acid.

Abbreviations List and Nomenclature

Abbreviations List

AOP	Advanced oxidation process
BPA	Bisphenol A
BPS	Bisphenol S
CE	Capillary electrophoresis
EDS	Energy dispersive X-ray spectroscopy
HRTEM	High resolution transmission electron microscopy
LAL	Laser ablation in liquids
LC/MS	Liquid chromatography coupled with mass spectroscopy
TEM	Transmission electron microscopy
TOC	Total organic carbon
SEM	Scanning electron microscopy

Nomenclature

$-r_{BPA,o}$	Initial BPA oxidation rate
k	Pseudo-first order kinetic constant
R2	Determination coefficient
CBPA,o	Initial BPA concentration
pHo	Initial pH
Wcat	Catalyst concentration

References

1. Chen, M.-Y.; Ike, M.; Fujita, M. Acute toxicity, mutagenicity, and estrogenicity of bisphenol-A and other bisphenols. *Environ. Toxicol.* **2002**, *17*, 80–86. [CrossRef] [PubMed]
2. Grignard, E.; Lapenna, S.; Bremer, S. Weak estrogenic transcriptional activities of Bisphenol A and Bisphenol S. *Toxicol. Vitr.* **2012**, *26*, 727–731. [CrossRef]
3. Zhu, S.; Khan, M.A.; Kameda, T.; Xu, H.; Wang, F.; Xia, M.; Yoshioka, T. New insights into the capture performance and mechanism of hazardous metals Cr^{3+} and Cd^{2+} onto an effective layered double hydroxide based material. *J. Hazard. Mater.* **2022**, *426*, 128062. [CrossRef] [PubMed]
4. Zhu, S.; Xia, M.; Chu, Y.; Khan, M.A.; Lei, W.; Wang, F.; Muhmood, T.; Wang, A. Adsorption and Desorption of Pb(II) on l-Lysine Modified Montmorillonite and the simulation of Interlayer Structure. *Appl. Clay Sci.* **2018**, *169*, 40–47. [CrossRef]
5. Munoz, M.; de Pedro, Z.M.; Casas, J.A.; Rodriguez, J.J. Preparation of magnetite-based catalysts and their application in heterogeneous Fenton oxidation—A review. *Appl. Catal. B Environ.* **2015**, *176–177*, 249–265. [CrossRef]
6. Chand, R.; Ince, N.H.; Gogate, P.R.; Bremner, D.H. Phenol degradation using 20, 300 and 520 kHz ultrasonic reactors with hydrogen peroxide, ozone and zero valent metals. *Sep. Purif. Technol.* **2009**, *67*, 103–109. [CrossRef]
7. Torres-Blancas, T.; Roa-Morales, G.; Barrera-Díaz, C.; Ureña-Nuñez, F.; Cruz-Olivares, J.; Balderas-Hernandez, P.; Natividad, R. Ozonation of Indigo Carmine Enhanced by Fe/Pimenta dioica L. Merrill Particles. *Int. J. Photoenergy* **2015**, *2015*, 608412. [CrossRef]
8. Ziylan, A.; Ince, N.H. Catalytic ozonation of ibuprofen with ultrasound and Fe-based catalysts. *Catal. Today* **2015**, *240*, 2–8. [CrossRef]
9. Umar, K.; Haque, M.M.; Mir, N.A.; Muneer, M.; Farooqi, I.H. Titanium Dioxide-mediated Photocatalysed Mineralization of Two Selected Organic Pollutants in Aqueous Suspensions. *J. Adv. Oxid. Technol.* **2013**, *16*, 252–260. [CrossRef]
10. Haque, M.M.; Khan, A.; Umar, K.; Mir, N.A.; Muneer, M.; Harada, T.; Matsumura, M. Synthesis, Characterization and Photocatalytic Activity of Visible Light Induced Ni-Doped TiO_2. *Energy Environ. Focus* **2013**, *2*, 73–78. [CrossRef]
11. Frankowski, R.; Płatkiewicz, J.; Stanisz, E.; Grześkowiak, T.; Zgoła-Grześkowiak, A. Biodegradation and photo-Fenton degradation of bisphenol A, bisphenol S and fluconazole in water. *Environ. Pollut.* **2021**, *289*, 117947. [CrossRef] [PubMed]
12. Huang, W.-C.; Jia, X.; Li, J.; Li, M. Dynamics of microbial community in the bioreactor for bisphenol S removal. *Sci. Total Environ.* **2019**, *662*, 15–21. [CrossRef] [PubMed]
13. Yang, T.; Wang, L.; Liu, Y.; Huang, Z.; He, H.; Wang, X.; Jiang, J.; Gao, D.; Ma, J. Comparative study on ferrate oxidation of BPS and BPAF: Kinetics, reaction mechanism, and the improvement on their biodegradability. *Water Res.* **2018**, *148*, 115–125. [CrossRef]
14. Chai, F.; Li, K.; Song, C.; Guo, X. Synthesis of magnetic porous Fe_3O_4/C/Cu_2O composite as an excellent photo-Fenton catalyst under neutral condition. *J. Colloid Interface Sci.* **2016**, *475*, 119–125. [CrossRef]
15. Davarnejad, R.; Azizi, J. Alcoholic wastewater treatment using electro-Fenton technique modified by Fe_2O_3 nanoparticles. *J. Environ. Chem. Eng.* **2016**, *4*, 2342–2349. [CrossRef]
16. Mahy, J.G.; Tasseroul, L.; Zubiaur, A.; Geens, J.; Brisbois, M.; Herlitschke, M.; Hermann, R.; Heinrichs, B.; Lambert, S.D. Highly dispersed iron xerogel catalysts for p-nitrophenol degradation by photo-Fenton effects. *Microporous Mesoporous Mater.* **2014**, *197*, 164–173. [CrossRef]

17. Dükkancı, M. Sono-photo-Fenton oxidation of bisphenol-A over a LaFeO$_3$ perovskite catalyst. *Ultrason. Sonochemistry* **2018**, *40*, 110–116. [CrossRef] [PubMed]

18. Noor, S.H.M.; Othman, M.H.D.; Khongnakorn, W.; Sinsamphanh, O.; Abdullah, H.; Puteh, M.H.; Kurniawan, T.A.; Zakria, H.S.; El-Badawy, T.; Ismail, A.F.; et al. Bisphenol A Removal Using Visible Light Driven Cu$_2$O/PVDF Photocatalytic Dual Layer Hollow Fiber Membrane. *Membranes* **2022**, *12*, 208. [CrossRef]

19. Chen, D.D.; Yi, X.H.; Ling, L.; Wang, C.C.; Wang, P. Photocatalytic Cr(VI) sequestration and photo-Fenton bisphenol A decomposition over white light responsive PANI/MIL-88A(Fe). *Appl. Organomet. Chem.* **2020**, *34*, e5795. [CrossRef]

20. Fu, H.; Song, X.X.; Wu, L.; Zhao, C.; Wang, P.; Wang, C.C. Room-temperature preparation of MIL-88A as a heterogeneous photo-Fenton catalyst for degradation of rhodamine B and bisphenol A under visible light. *Mater. Res. Bull.* **2020**, *125*, 110806. [CrossRef]

21. Huang, W.; Luo, M.; Wei, C.; Wang, Y.; Hanna, K.; Mailhot, G. Enhanced heterogeneous photo-Fenton process modified by magnetite and EDDS: BPA degradation. *Environ. Sci. Pollut. Res.* **2017**, *24*, 10421–10429. [CrossRef] [PubMed]

22. Pérez-Moya, M.; Kaisto, T.; Navarro, M.; del Valle, L.J. Study of the degradation performance (TOC, BOD, and toxicity) of bisphenol A by the photo-Fenton process. *Environ. Sci. Pollut. Res.* **2016**, *24*, 6241–6251. [CrossRef]

23. Silva, L.G.R.; Costa, E.P.; Starling, M.C.V.M.; Azevedo, T.d.S.; Bottrel, S.E.C.; Pereira, R.O.; Sanson, A.L.; Afonso, R.J.C.F.; Amorim, C.C. LED irradiated photo-Fenton for the removal of estrogenic activity and endocrine disruptors from wastewater treatment plant effluent. *Environ. Sci. Pollut. Res.* **2021**, *28*, 24067–24078. [CrossRef] [PubMed]

24. Xiao, S.; Zhou, C.; Ye, X.; Lian, Z.; Zhang, N.; Yang, J.; Chen, W.; Li, H. Solid-Phase Microwave Reduction of WO$_3$ by GO for Enhanced Synergistic Photo-Fenton Catalytic Degradation of Bisphenol A. *ACS Appl. Mater Inter.* **2020**, *12*, 32604–32614. [CrossRef] [PubMed]

25. Khandarkhaeva, M.; Batoeva, A.; Sizykh, M.; Aseev, D.; Garkusheva, N. Photo-Fenton-like degradation of bisphenol A by persulfate and solar irradiation. *J. Environ. Manag.* **2019**, *249*, 109348. [CrossRef]

26. Liu, Y.; Mao, Y.; Tang, X.; Xu, Y.; Li, C.; Li, F. Synthesis of Ag/AgCl/Fe-S plasmonic catalyst for bisphenol A degradation in heterogeneous photo-Fenton system under visible light irradiation. *Chin. J. Catal.* **2017**, *38*, 1726–1735. [CrossRef]

27. Bremner, D.H.; Burgess, A.E.; Houllemare, D.; Namkung, K.-C. Phenol degradation using hydroxyl radicals generated from zero-valent iron and hydrogen peroxide. *Appl. Catal. B: Environ.* **2006**, *63*, 15–19. [CrossRef]

28. Cheng, R.; Cheng, C.; Liu, G.-H.; Zheng, X.; Li, G.; Li, J. Removing pentachlorophenol from water using a nanoscale zero-valent iron/H$_2$O$_2$ system. *Chemosphere* **2015**, *141*, 138–143. [CrossRef]

29. Machado, S.; Stawiński, W.; Slonina, P.; Pinto, A.R.; Grosso, J.P.; Nouws, H.P.A.; Albergariaa, J.T.; Delerue-Matosa, C. Application of green zero-valent iron nanoparticles to the remediation of soils contaminated with ibuprofen. *Sci. Total Environ.* **2013**, *461–462*, 323–329. [CrossRef]

30. de la Plata, G.B.O.; Alfano, O.M.; Cassano, A.E. 2-Chlorophenol degradation via photo Fenton reaction employing zero valent iron nanoparticles. *J. Photochem. Photobiol. A: Chem.* **2012**, *233*, 53–59. [CrossRef]

31. Pastrana-Martínez, L.M.; Pereira, N.; Lima, R.; Faria, J.L.; Gomes, H.T.; Silva, A.M.T. Degradation of diphenhydramine by photo-Fenton using magnetically recoverable iron oxide nanoparticles as catalyst. *Chem. Eng. J.* **2015**, *261*, 45–52. [CrossRef]

32. Shahwan, T.; Abu Sirriah, S.; Nairat, M.; Boyacı, E.; Eroğlu, A.; Scott, T.; Hallam, K. Green synthesis of iron nanoparticles and their application as a Fenton-like catalyst for the degradation of aqueous cationic and anionic dyes. *Chem. Eng. J.* **2011**, *172*, 258–266. [CrossRef]

33. Shin, S.; Yoon, H.; Jang, J. Polymer-encapsulated iron oxide nanoparticles as highly efficient Fenton catalysts. *Catal. Commun.* **2008**, *10*, 178–182. [CrossRef]

34. Morales-Leal, F.J.; De la Rosa, J.R.; Lucio-Ortiz, C.J.; Martínez, D.B.; Rio, D.A.D.H.D.; Garza-Navarro, M.A.; Martínez-Vargas, D.X.; Garcia, C.D. Comparison between the catalytic and photocatalytic activities of Cu/Al$_2$O$_3$ and TiO$_2$ in the liquid–phase oxidation of methanol–ethanol mixtures: Development of a kinetic model for the preparation of catalyst. *Appl. Catal. A Gen.* **2018**, *562*, 184–197. [CrossRef]

35. Pradhan, A.C.; Parida, K.M.; Nanda, B. Enhanced photocatalytic and adsorptive degradation of organic dyes by mesoporous Cu/Al$_2$O$_3$–MCM-41: Intra-particle mesoporosity, electron transfer and OH radical generation under visible light. *Dalton. T.* **2011**, *40*, 7348–7356. [CrossRef]

36. Javaid, R.; Qazi, U.Y. Catalytic Oxidation Process for the Degradation of Synthetic Dyes: An Overview. *Int. J. Environ. Res. Public Health* **2019**, *16*, 2066. [CrossRef]

37. Kanitz, A.; Kalus, M.-R.; Gurevich, E.L.; Ostendorf, A.; Barcikowski, S.; Amans, D. Review on experimental and theoretical investigations of the early stage, femtoseconds to microseconds processes during laser ablation in liquid-phase for the synthesis of colloidal nanoparticles. *Plasma Sources Sci. Technol.* **2019**, *28*, 103001. [CrossRef]

38. Rehbock, C.; Merk, V.; Gamrad, L.; Streubel, R.; Barcikowski, S. Size control of laser-fabricated surfactant-free gold nanoparticles with highly diluted electrolytes and their subsequent bioconjugation. *Phys. Chem. Chem. Phys.* **2012**, *15*, 3057–3067. [CrossRef]

39. Olea-Mejía, O.; Fernández-Mondragón, M.; Rodríguez-de la Concha, G.; Camacho-López, M. SERS-active Ag, Au and Ag–Au alloy nanoparticles obtained by laser ablation in liquids for sensing methylene blue. *Appl. Surf. Sci.* **2015**, *348*, 66–70. [CrossRef]

40. Eisenberg, G. Colorimetric Determination of Hydrogen Peroxide. *Ind. Eng. Chem. Anal. Ed.* **1943**, *15*, 327–328. [CrossRef]

41. Amado-Piña, D.; Roa-Morales, G.; Molina-Mendieta, M.; Balderas-Hernández, P.; Romero, R.; Díaz, C.E.B.; Natividad, R. E-peroxone process of a chlorinated compound: Oxidant species, degradation pathway and phytotoxicity. *J. Environ. Chem. Eng.* **2022**, *10*, 108148. [CrossRef]

42. Alvarado-Rolon, O.; Natividad, R.; Ramírez-García, J.; Orozco-Velazco, J.; Hernandez-Servin, J.; Ramírez-Serrano, A. Kinetic modelling of paracetamol degradation by photocatalysis: Incorporating the competition for photons by the organic molecule and the photocatalyst. *J. Photochem. Photobiol. A Chem.* **2021**, *412*, 113252. [CrossRef]

43. Brillas, E.; Sirés, I.; Oturan, M.A. Electro-Fenton Process and Related Electrochemical Technologies Based on Fenton's Reaction Chemistry. *Chem. Rev.* **2009**, *109*, 6570–6631. [CrossRef] [PubMed]

44. Hurtado, L.; Romero, R.; Mendoza, A.; Brewer, S.; Donkor, K.; Gómez-Espinosa, R.M.; Natividad, R. Paracetamol mineralization by Photo Fenton process catalyzed by a Cu/Fe-PILC under circumneutral pH conditions. *J. Photochem. Photobiol. A Chem.* **2019**, *373*, 162–170. [CrossRef]

45. Hurtado, L.; Avilés, O.; Brewer, S.; Donkor, K.K.; Romero, R.; Gómez-Espinosa, R.M.; Alvarado, O.; Natividad, R. Al/Cu-PILC as a Photo-Fenton Catalyst: Paracetamol Mineralization. *ACS Omega* **2022**, *7*, 23821–23832. [CrossRef] [PubMed]

46. Watanabe, N.; Horikoshi, S.; Kawabe, H.; Sugie, Y.; Zhao, J.; Hidaka, H. Photodegradation mechanism for bisphenol A at the TiO$_2$/H$_2$O interfaces. *Chemosphere* **2003**, *52*, 851–859. [CrossRef]

47. Bechambi, O.; Jlaiel, L.; Najjar, W.; Sayadi, S. Photocatalytic degradation of bisphenol A in the presence of Ce–ZnO: Evolution of kinetics, toxicity and photodegradation mechanism. *Mat. Chem. Phys.* **2016**, *173*, 95–105. [CrossRef]

48. Young, T.; Geng, M.; Thagard, S.M.; Lin, L. Oxidative Degradation of Bisphenol A: A Comparison Between Fenton Reagent, UV, UV/H$_2$O$_2$ and Ultrasound. *J. Adv. Oxid. Technol.* **2013**, *16*, 89–101. [CrossRef]

49. Mendoza, A.; Romero, R.; Gutiérrez-Cedillo, G.P.; López-Tellez, G.; Lorenzo-González, O.; Gómez-Espinosa, R.M.; Natividad, R. Selective production of dihydroxyacetone and glyceraldehyde by photo-assisted oxidation of glycerol. *Catal. Today* **2019**, *358*, 149–154. [CrossRef]